ULTRAVIOLET SPECTROMETER EXPERIMENT FOR THE VOYAGER MISSION

A. L. BROADFOOT, B. R. SANDEL and D. E. SHEMANSKY
Kitt Peak National Observatory, Tucson, Ariz. 85726, U.S.A.

S. K. ATREYA and T. M. DONAHUE
University of Michigan, Ann Arbor, Mich. 48109, U.S.A.

H. W. MOOS
Johns Hopkins University, Baltimore, Md 21218, U.S.A.

J. L. BERTAUX and J. E. BLAMONT
Service d'Aeronomie du CNRS, Paris, France

J. M. AJELLO
Jet Propulsion Laboratory, Pasadena, Calif. 91103, U.S.A.

D. F. STROBEL
Naval Research Laboratory, Washington, D.C. 20375, U.S.A.

J. C. McCONNELL
York University, Ontario M3J 1P3, Canada

and

A. DALGARNO, R. GOODY, M. B. McELROY, and Y. L. YUNG
Harvard University, Cambridge, Mass. 02138, U.S.A.

(Received 24 May, 1977)

Abstract. The Voyager Ultraviolet Spectrometer (UVS) is an objective grating spectrometer covering the wavelength range of 500–1700 Å with 10 Å resolution. Its primary goal is the determination of the composition and structure of the atmospheres of Jupiter, Saturn, Uranus and several of their satellites. The capability for two very different observational modes have been combined in a single instrument. Observations in the airglow mode measure radiation from the atmosphere due to resonant scattering of the solar flux or energetic particle bombardment, and the occultation mode provides measurements of the atmospheric extinction of solar or stellar radiation as the spacecraft enters the shadow zone behind the target. In addition to the primary goal of the solar system atmospheric measurements, the UVS is expected to make valuable contributions to stellar astronomy at wavelengths below 1000 Å.

1. Introduction

The primary goal of the Ultraviolet Spectrometer experiment is to determine the composition and structure of the atmospheres of Jupiter, Saturn, and their satellites. We may also have the opportunity to examine the Uranus system. These planets are expected to have qualitatively similar atmospheres consisting of H, H_2, He and CH_4. A typical model atmosphere for Jupiter (Atreya and Donahue, 1976) is shown in Figure 1. Of particular interest are the mixing ratios of H_2 and He in the mixed

Space Science Reviews **21** (1977) 183–205.

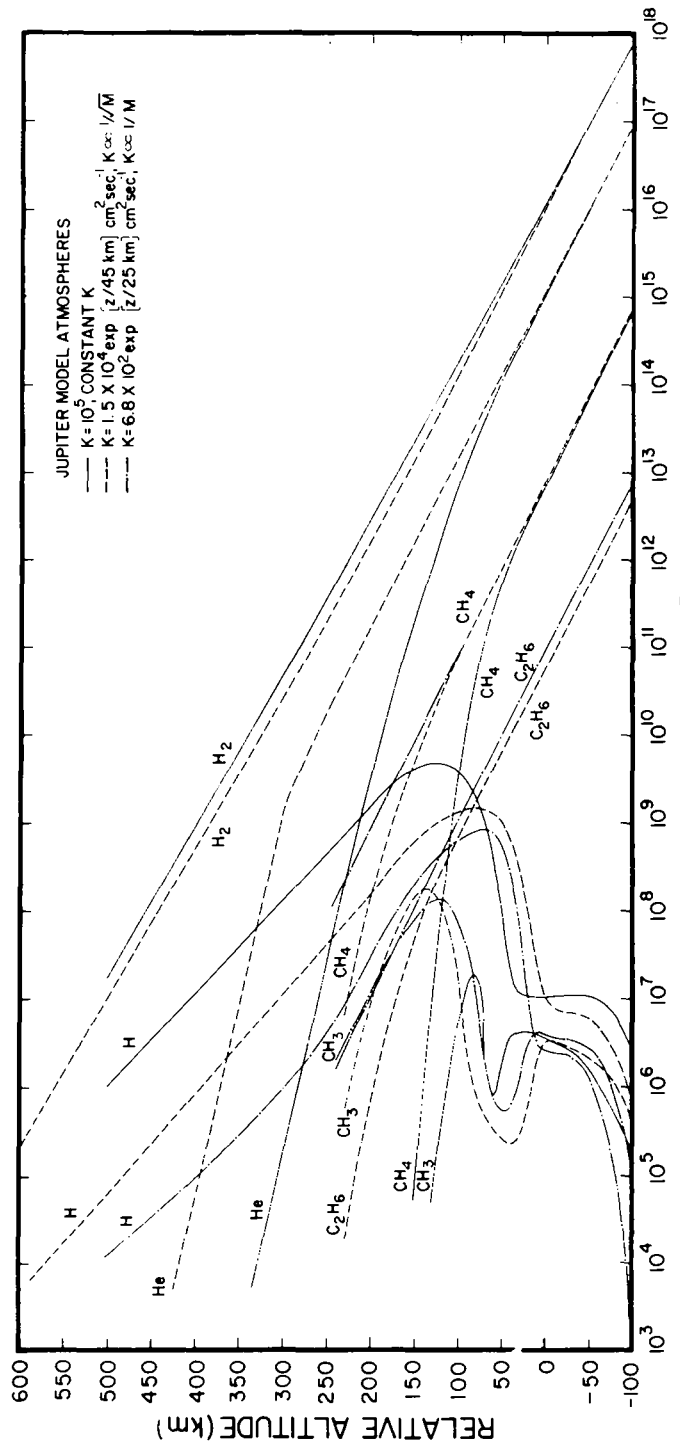

Fig. 1. Model atmospheres for Jupiter taken from Atreya and Donahue (1976). These models are based on the assumption of a He/H_2 ratio of 0.1 and an exosphere temperature of 150 K. The reference altitude is at the 10^{16} cm^{-3} number density level.

portion of the atmospheres and the thermal structure of the thermosphere, mesosphere and stratosphere. Information on the nature of the Jovian magnetosphere and its trapped particles can be inferred from observations of the particle interactions with the atmospheres of Jupiter and the Galilean satellites. Mapping the entire region of space associated with the Galilean satellites is important in understanding the mechanisms for the production and maintenance of gaseous tori associated with the satellites. The distribution of hydrogen and helium in the heliosphere, inferred from high resolution maps of the celestial sphere, will lead to a better understanding of the interaction between the solar system and the interstellar wind. Finally, the first prolonged exploratory astronomical observations at wavelengths shorter than 1000 Å will be possible.

The low exospheric temperatures and the large gravitational potential barrier of the outer planets have retarded the escape of even the lightest gases from their atmospheres. Even the relatively high temperatures now inferred for the thermosphere and exosphere of Jupiter (Atreya and Donahue, 1976; Fjeldbo *et al.*, 1976) are far too low to permit thermal escape of hydrogen. Therefore, the chemical composition of the atmospheres probably reflect the conditions of the primordial solar nebula. The knowledge of the conditions when this part of the solar system was formed is essential to the understanding of the origin and evolution of the solar system. In particular, the ratio of helium to hydrogen abundances in the major planets is a datum of considerable significance. These quantities are also important in the formulation of model atmospheres of the planets. Of greatest interest is a measurement of the distribution of H, H_2, and He throughout as much of the atmosphere as possible, but especially below the homopause where strong mixing occurs. For many problems the significant quantity is the planetary abundance ratio rather than the ratio in the regions of gravitational separation above the homopause where molecular diffusion, rather than mechanical stirring, controls the distribution of individual gas species. Thus, an accurate determination of the altitude of the homopause is of crucial importance.

Several features of Jupiter's atmosphere observed by ground-based, rocket and satellite instruments have raised questions in the past several years. Interpretation of structure and the light curve obtained in the β Sco occultation (Veverka *et al.*, 1974; French and Gierasch, 1974) on the basis of upward propagating gravity waves (Atreya and Donahue, 1976) leads to the conclusion that thermospheric temperatures should be higher than can be expected from the absorption of solar UV radiation and an internal heat source. This suggests that there is an additional energy source for heating the upper atmosphere of the giant planets. An unambiguous determination of the temperature profile in the upper atmosphere is needed to guide models for this heat source. Measurements of the Ly-α brightness have yielded values ranging over an order of magnitude, from 400 to 4000 Rayleighs (Moos *et al.*, 1969; Giles *et al.*, 1976; Barker, 1977, Rottman *et al.*, 1973; Carlson and Judge, 1974). Since resonance scattering of sunlight is expected to contribute only about 1 kR of Ly-α, the higher intensities sometimes observed tend to confirm the higher

atmospheric temperatures. It has not been possible to determine whether or not a portion of the source is localized on the disk of the planet. Rocket observations of Jupiter (Giles *et al.*, 1976) have detected weak emissions between ~1250 and ~1500 Å, which are tentatively identified as emissions from H_2 Lyman bands excited by low energy electrons.

Such auroral-type excitation of atmospheric constituents is expected to provide information on the bombarding electron fluxes and energy distributions. The results may contribute significantly to the understanding of atmosphere-magnetosphere interactions and the coupling of satellites, particularly Io, and Jupiter via the magnetosphere. Based on an analysis of the Io-magnetosphere interaction by Goldreich and Lynden-Bell (1969), large energy fluxes are expected to be deposited in the atmosphere of Jupiter at the foot of the Io flux tube. Several hundred kR of Ly-α emission is expected to originate from the northern as well as the southern foot of the flux tube. This radiation will be easily observable on the darkside of Jupiter. The measurement of the Ly-α emission from the hot spots will provide valuable information on the nature and intensity of the electron flux in the flux tube, the configuration of the Jovian magnetic field, and probably on the upper atmosphere of Jupiter. We also expect to learn about the correlation between the flux tube and the sodium emission from Io's torus. Although such correlation has not been firmly established, there are indications that such a relation might exist (Trafton and Macy, 1975). On Io, both proton and electron auroras are expected (Pilcher, 1976).

Another satellite-related phenomenon of interest is the gas cloud associated with Io, and possibly other Galilean satellites. Io's Sodium D line emission has been shown to extend to the space around Io (Trafton *et al.*, 1974). The Pioneer 10 UV photometer detected a UV emission, probably resonantly scattered Ly-α, from a region of Io's orbit approximately centered on the satellite (Carlson and Judge, 1975). A complete map of the satellite system in the UV will establish unambiguously the identity and spatial distribution of the scattering species and detect similar emissions associated with other satellites if they are present. Adequate information should be available to determine the production rate of the scattering species, which presumably originate at the surface of the satellite. This should lead to an understanding of the mechanism of production.

The UVS will be the first spectrometer capable of prolonged stellar observations in the wavelength range of 500 to 1000 Å, and the only one expected to be operational for several years. Therefore, a tremendous exploratory potential exists. Rocket-borne spectrometers have recently identified several extreme UV sources (Lampton *et al.*, 1976). These fascinating discoveries require further information, but no comprehensive survey will be possible until the Voyager Mission. In addition to discrete sources, the UV continuum of the cosmic background radiation is expected to be measurable.

As the solar system moves through the local neutral interstellar medium, the interstellar medium penetrates the heliosphere as the interstellar wind. The distribution of the constituents of the interstellar medium, primarily hydrogen and helium, is

determined by the combined effects of solar gravitation and radiation pressure, and the rate of relevant ionization processes (Blum *et al.*, 1975). In the case of neutral helium, solar gravitational forces dominate radiation pressure forces and the atoms are focused on the downstream side of the sun, leading to a maximum in the intensity of resonantly-scattered He 584 Å radiation. For hydrogen, however, these forces are more nearly balanced and the effect varies with solar radiation pressure. Measurements of the column densities of He and H can provide information on the density and velocity of the interstellar wind. Gravitational focusing of hydrogen by Jupiter itself will be easily observable.

2. Instrument Description

The Voyager Ultraviolet Spectrometer is an objective grating spectrometer covering the wavelength range of 500–1700 Å in 128 contiguous intervals. A photograph of the instrument is shown in Figure 2, and an optical diagram is shown in Figure 3.

2.1. Optical configuration

An objective grating spectrometer is commonly used for observations of point sources. This instrument was adapted to observe extended emission sources by restricting the field of view in the dispersive direction sufficiently to provide broad spectral separation of emission in the image plane. An open, or reflective, optical system is required to allow transmission of wavelengths short of 1050 Å, the shortest wavelength transmitted by a solid. Reflective efficiencies are very low at these short wavelengths, except for grazing incidence, and restrict a practical instrument to a single reflection for weak emissions. The field of view was restricted with a series of precision mechanical stops which we refer to as the 'collimator' since it controls the illumination of the grating which then has the optical properties described by Wadsworth (1896) (see also Beutler, 1945). The collimator was designed to minimize Fresnel diffraction, but the mechanical structure does represent a substantial loss in aperture, about two-thirds, and has scattering characteristics which compromise the spectrum to some extent. In practice, separation of significant spectral and background features is a reasonably tractable process, particularly for weak emission lines.

The collimator restricts the field of view in the dispersion direction of the grating to 0.1° FWHM, but is essentially open in the cross-dispersion direction; the field of view in this long direction is defined by the angular width of the detector in the image plane and is about 0.87°. The diffraction grating is a platinum replica with a radius of curvature of 400.1 mm. It was custom-ruled in gold with 10 panels which were required to give a blaze wavelength of 800 Å on a 40×60 mm blank. A plate dispersion of 93 Å/mm was required to match the spectral range to the detector and thus we have a ruling of 540 lines/mm.

The instrument has two distinctly different spatial and spectral resolutions depending on the nature of the source. (1) An extended line-emission source, which

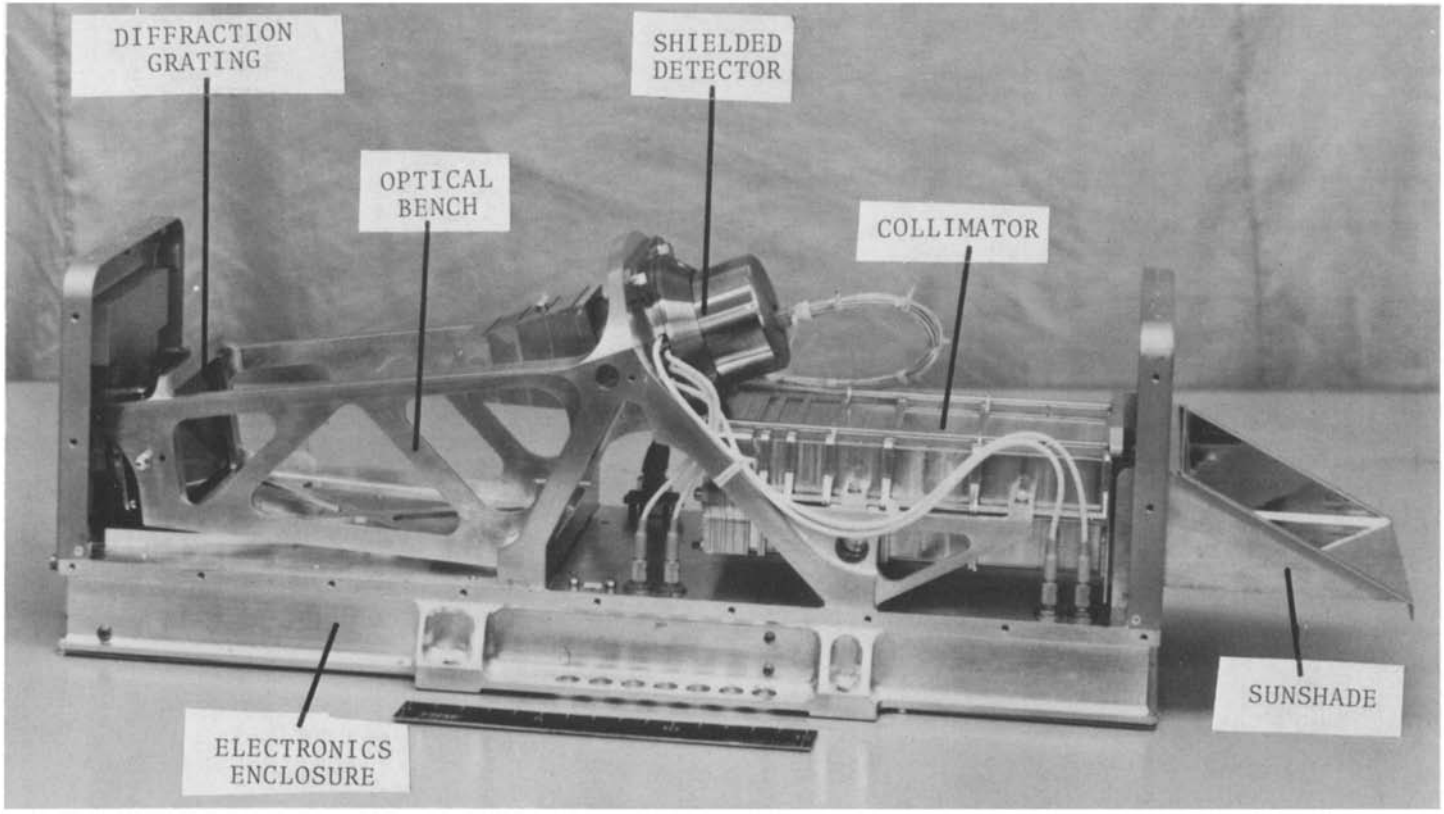

Fig. 2. A photograph of the Ultraviolet Spectrometer with the protective cover removed from the optical section. The optical bench supports the grating, the copper and aluminum detector housing, and a box-like structure containing the etched plates forming the mechanical collimator. Most of the electronics are housed in the base with access through the bottom. This design minimizes contamination of the optical section by outgassing.

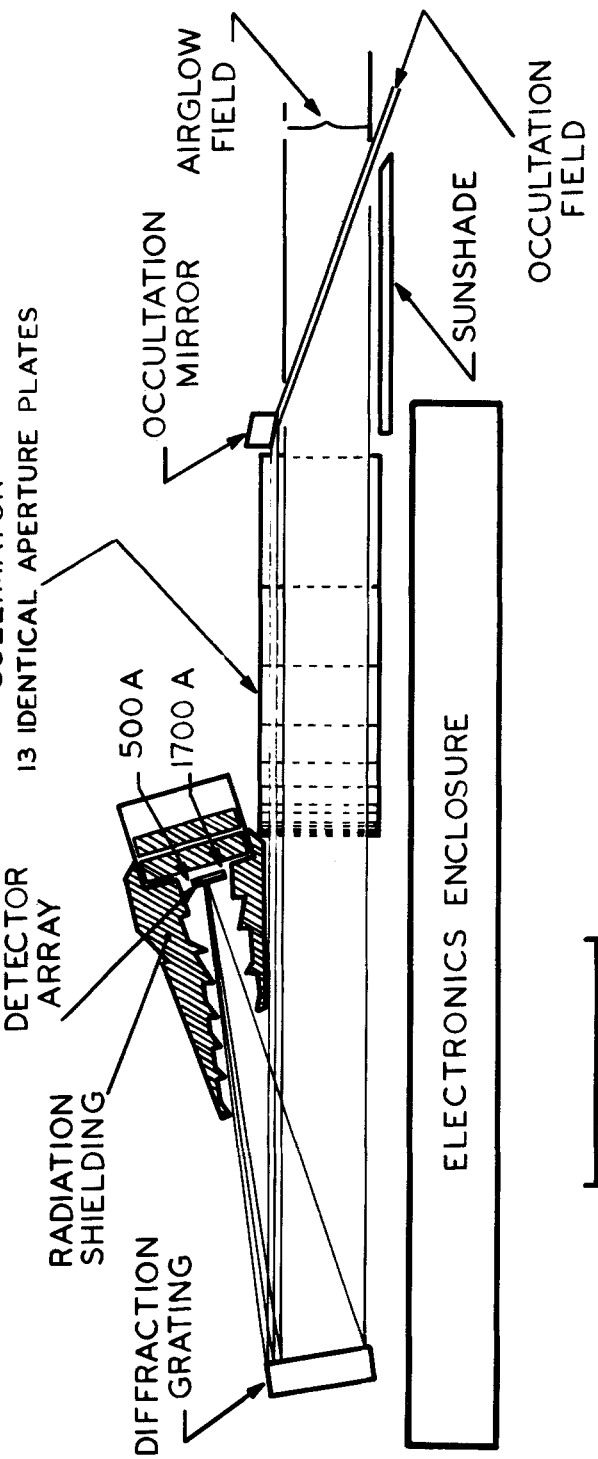

Fig. 3. A simplified optical diagram of the UVS. The occultation field of view is offset 20° with respect to the larger airglow field of view by a reflection at the occultation mirror. The path of the fields are then parallel through the collimator to the concave grating. The grating disperses wavelengths and images the fields on the detector array.

fills the field of view of the instrument, produces a triangular intensity distribution in the image plane 0.1° in half-width; that is a spectral half-width of 33 Å. (2) A point source is accurately imaged in the image plane and the width of a detector element, 0.029°, provides both the spectral and spatial parameter. But spatial and spectral resolution may be improved to some extent through spectral analysis.

An auxiliary field of view for the solar occultation experiment is offset 20° from the main field of view so that the UVS and other scan platform instruments boresighted with the UVS will not be pointed towards the Sun during that experiment. An aluminum mirror directs the solar radiation through a special 0.75 cm^2 aperture in the collimator, as shown in Figure 3. A sunshade protects the main aperture from direct solar rays during this experiment. Photometrically, the occultation and airglow apertures are related in the ratio 1 : 19; no dark slide is provided for the occultation port and we must maintain cognizance of possible spectral contamination during airglow experiments.

2.2. Detector

The photon counting detector utilizes a 128-element linear self-scanned anode array to collect the output of a dual microchannel plate (MCP) electron multiplier. This detector was developed for this instrument and has been described by Broadfoot and Sandel (1977); the acronym Ssanacon has been adopted for this detector since the self-scanned anode array is a unique device. The 128 narrow aluminum anodes, each 3 mm long, are deposited on 0.1 mm centers for a total collecting length of 13 mm. The specially designed 18 mm diameter MCP's have a rectangular active area corresponding to the collecting area of the anode array. The makeup of the detector is illustrated in Figure 4. Photons diffracted by the grating to the detector produce photoelectrons in one of two ways, either from the surface of the MCP or from a semi-transparent photocathode in proximity to the MCP. The CuI photocathode is deposited on a MgF_2 filter plate to extend the response of the detector to 1700 Å, where the MCP quantum efficiency is very low. A hole in the filter plate allows wavelengths shorter than 1250 Å to fall directly on the MCP surface. The MgF_2 filter also serves as an order sorting filter.

Photoelectrons undergo about 10^6 amplification through the cascaded microchannel plates. The pulse of electrons falls on the self-scanned anode array where the charge is stored. The anodes are accessed sequentially by a shift register and FET switches contained in the single integrated circuit. The scanning circuitry discharges each anode into a charge sensitive amplifier. The charge pulse is processed and the information added into a shift register memory consisting of 128 16-bit words. The memory location is synchronized to the scanning of the anode array so that there is a one-to-one correspondence between anode and memory location. The 128-anode array is really two separate interdigitated 64-anode arrays scanned by two shift registers. The shift registers and memories are driven by a 200 kHz clock, so that an individual anode is accessed every 320 μsec.

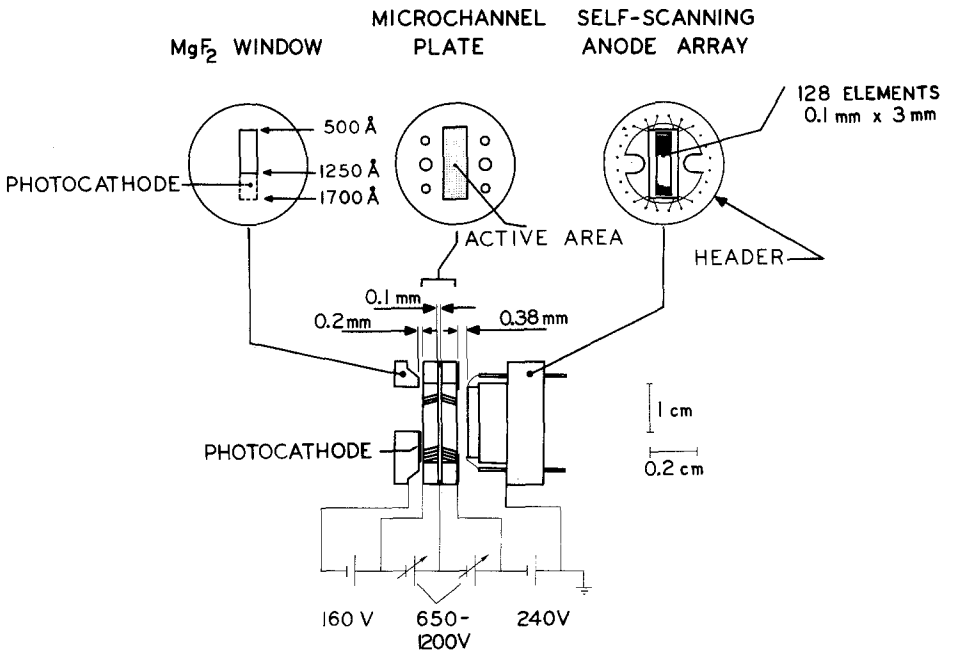

Fig. 4. The UV detector components.

Two modes of electrical operation allow the detector to operate in a photon-counting mode for low source intensities, or in an integration model for high source intensities. In the pulse counting mode the number in the appropriate memory location is incremented by one if a charge above a fixed threshold is detected on an anode. The access time of 320 μsec implies that single random photon events can be recorded on any one of the 128 anodes with a rate of about 300 per second on each anode with a coincidence loss of about 10% of the events; such a loss can be corrected statistically. This is a satisfactorily high rate for the weak emissions which we anticipate in the airglow mode.

In the integration mode, a 3-bit analog-to-digital converter is introduced ahead of the adder. In this case the charge on the diode is coarsely digitized and added to the previous accumulated charge preserved digitally in the memory. The statistics of sampling these events is complicated by the logarithmic pulse height distribution of the events. There is also a logarithmic current limit function of the MCP's at these high event rates. The seventh level of the A-to-D converter has been adjusted to correspond to about 10 average pulse events which have been logarithmically compressed by the current limit characteristics of the MCP. The gain of the microchannel plate is adjustable by 7 steps of high voltage and can be adjusted to allow the seventh level to correspond to a wide range of event rates depending on the emission intensity. It can be shown that the statistics of the high rate signals are maintained by this technique. Absolute calibration of this approach is not very

practical; however, it should be noted that this mode is used for the occultation experiment in which we are only interested in the change of intensity with about a 1% accuracy. Calibration and adjustment for this experiment will be performed in flight.

2.3. Data Rates

As explained above, the anode array is scanned continuously at a 3 kHz rate, and the data are digitized and added into the instrument's memory. On command from the flight data system (FDS), a pair of UVS data words is transferred to the FDS, compressed from 16 to 10 bits, and transmitted or stored on the spacecraft. The spectral integration time in the instrument is therefore determined by the spacecraft's FDS, which can interrogate the memory and transfer the spectral data at various rates depending on the phase of the mission and experimental requirements. The highest data rate, which is used for the occultation experiments, is 4 kbit/sec corresponding to the transfer of one complete spectrum in 0.32 sec. For airglow measurements near encounter, a spectrum will be transferred in 3.84 sec. In the cruise mode, a spectrum can be accumulated in the instrument memory for several hours, and then transmitted at an available bit rate.

2.4. Sensitivity

The counting rate summed over all channels for a 1 Rayleigh monochromatic source filling the field of view is given by the photometric equation

$$P = K\omega A\eta_1\eta_2(\lambda)\eta_3(\lambda) = KS_\lambda,$$

where P = counting rate in counts s^{-1} R^{-1},
$K = 10^6/4\pi$ photons cm^{-2} s^{-1} sr^{-1} R^{-1},
ω = angular field of view of the airglow port, $0.87° \times 0.2°$, or 5.3×10^{-5} steradian,
A = ruled area of the grating illuminated by the airglow aperture, 21.2 cm^2,
η_1 = transmission of the collimator, 0.33,
$\eta_2(\lambda)$ = grating efficiency, and
$\eta_3(\lambda)$ = detector quantum efficiency.

The sensitivity as a function of wavelength for this geometry (a uniform, extended monochromatic source filling the field of view) is shown by the solid line in Figure 5. The discontinuity at 1400 Å is due to the presence of the photocathode over the long wavelength portion of the spectrum. Because of the triangular transmission function of the collimator, radiation from a monochromatic extended source incident on the detector will fall in a triangular intensity distribution over 7 anodes. The triangular half-width of 3.5 anodes will receive 75% of the signal. For an extended source emitting a continuum of wavelengths with brightness 1 R/Å, the count rate for a single anode is given by

$$P = KWS_\lambda,$$

where W = spectral half-width, 33 Å.

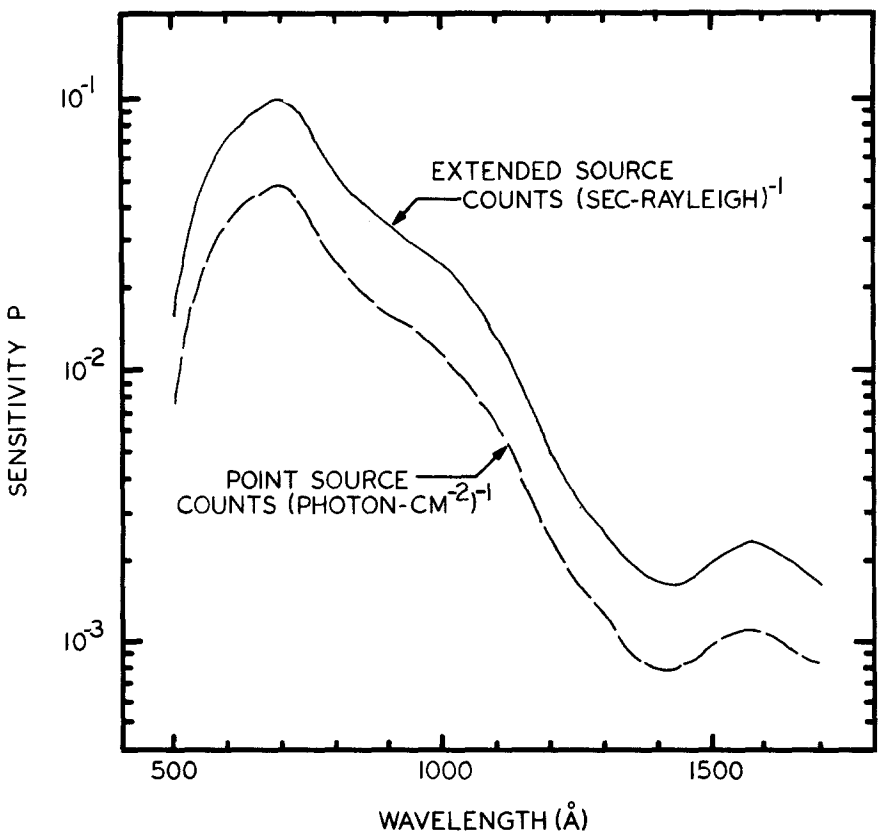

Fig. 5. Sensitivity of the UVS as a function of wavelength for two different observing geometries.

Monochromatic emission from a point source is imaged on an area much smaller than an anode width. For this case, the count rate is given by

$$P = \Phi A \eta_4 \eta_2(\lambda) \eta_3(\lambda),$$

where Φ = photon flux from the source (cm^{-2} s^{-1}),

η_4 = transmission of the collimator for a point source on the optic axis, 0.66,

and the other symbols have the same definition as above. The count rate for a source flux of 1 photon cm^{-2} s^{-1} as a function of wavelength is shown by the dashed curve in Figure 5. For an off-axis source, the signal rate will be reduced by the triangular transmission function of the collimator.

The practical lower limit for the signal measurable by the UVS instrument is a function of both the instrument sensitivity and the dark count rate of the detector. An important advantage of the Ssanacon is its extremely low intrinsic dark count rate of less than 3×10^{-3} count anode^{-1} s^{-1}. As an example, for radiation at the wavelength of peak sensitivity, a 20 min integration period yields 12 signal counts from a source intensity of 0.1 R. The square root of the number of dark counts recorded over the

same time period is 3; detection of the signal is unambiguous. As an astronomical instrument, the ultraviolet spectrometer compares favorably with other space spectrometers.

When the spacecraft is within about $15R_J$ of Jupiter, noise induced by high energy electrons trapped in the Jovian magnetic field greatly exceeds the intrinsic noise of the detector. Extensive shielding has been provided around the detector to reduce radiation interference.

The most sensitive element of the detector is the microchannel plate electron multiplier; its detection efficiency for high energy electrons has been measured and a shielding design has been developed that will allow the UVS to accumulate useful

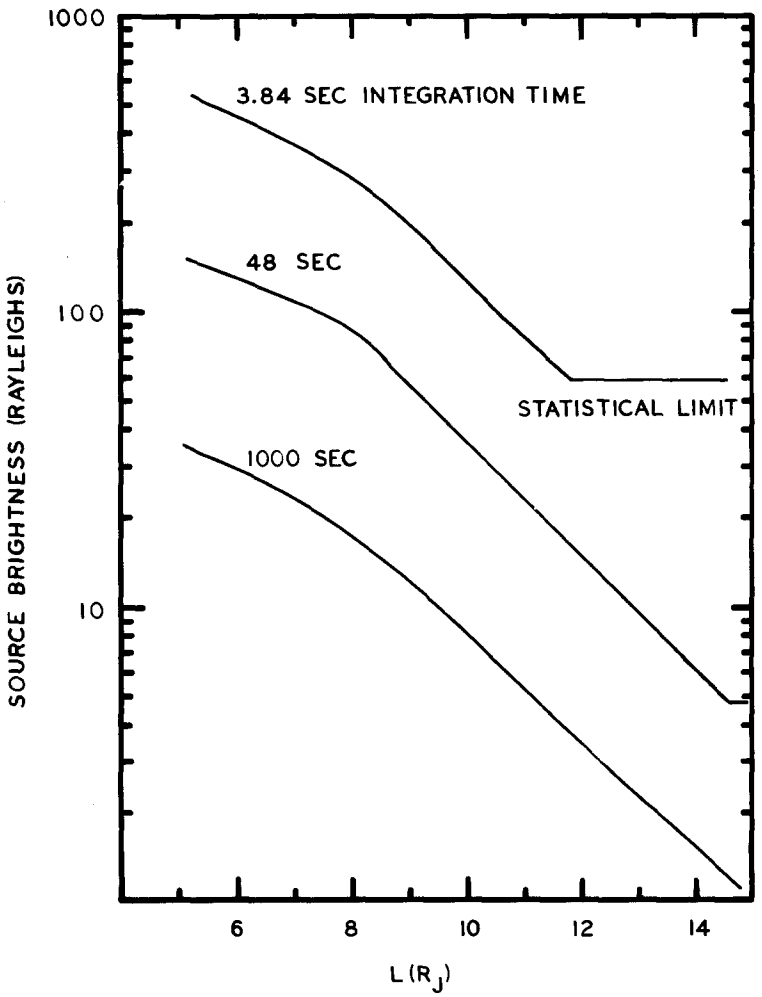

Fig. 6. Minimum detectable signal as a function of the McIlwain L parameter for several integration times. The horizontal portion of the curves represent a limitation due to counting statistics rather than radiation noise. These curves are appropriate for radiation at the wavelength of peak UVS sensitivity, about 700 Å.

data at the closest approach of the proposed Voyager trajectory to Jupiter. This shield is composed of approximately 1.25 kg of copper and aluminum distributed to obtain a sphere of 14 g cm^{-2} thickness over 95% of a sphere viewed from the detector, with less shielding over the remaining open aperture chosen so that the shielding effectiveness versus mass trade-off is optimized.

Figure 6 shows the minimum detectable signal as a function of the McIlwain L parameter for several signal integration times. These curves are based on the flux of electrons and Bremsstrahlung γ rays through the detector shielding assuming the JPL January 76 radiation model. The minimum detectable signal is defined as either: (a) the signal required to produce 25 signal counts in the integration time (20% statistics) or, (b) the signal required to produce a number of signal counts equal to $3\sqrt{}$(noise counts) in the integration time, whichever is larger. These curves are appropriate for an extended source filling the field of view, and for radiation at the wavelength of peak sensitivity, about 700 Å. Even at $5R_J$, the UVS can distinguish a 150 R signal given a rather modest 48 sec integration time; at $L > 14R_J$ the instrument sensitivity, rather than radiation noise, is the factor limiting the minimum detectable signal.

3. Remote Observations of Planetary Atmospheres

Two fundamentally different techniques are available to the UVS for remote spectroscopic probing of a planetary atmosphere: airglow and occultation. These techniques actually require two different types of spectrometers to perform the observations, one with a large collecting area for maximum sensitivity to weak emissions, and one that can look directly at the Sun and monitor solar emission intensities with high statistical accuracy. Both of these instruments have been combined to take advantage of a common detector system. Indeed, two entirely different instruments were constructed for these experiments for the Mariner 10 Mission (Broadfoot *et al.*, 1977a; Broadfoot *et al.*, 1977b). The airglow spectrum will provide an identification of the radiating components of the atmosphere and their absolute intensities. The field of view is small enough that the distribution of intensity through the planet-satellite system can be measured; at close approach the intensity can be measured as a function of altitude in the atmosphere to infer the scale height of the radiating species. The distribution of intensity over the object can also be determined. The occultation experiment uses the Sun as a source of UV radiation to measure the extinction properties of the atmosphere as the spacecraft moves into the planetary shadow; this is an important tool for the determination of the atmospheric structure.

3.1. Airglow observation

At Jupiter, H Ly-α emission will be excited in the upper atmosphere by resonance scattering of solar radiation by atomic hydrogen and by photodissociative excitation of molecular hydrogen. Emission will also be excited by electron and proton

bombardment of the atmosphere. These sources of emission can be separated through the spectral analysis. We can describe some of the expected emissions by use of atmospheric models and assumed excitations (Atreya and Donahue, 1976). Viewed along the optical paths perpendicular to the Jupiter–Sun axis, H Ly-α resonance scattering will produce an emission rate increasing from about 100 R, 1000 km above the turbopause to about 5 kR close to the limb. Because of the large geometrical amplification factor, photodissociation of molecular hydrogen should produce a signal rising rapidly from 10 R at 400 km to a maximum of about 10 kR near 250 km, and then decreasing rapidly again below 1 kR at lower altitudes. This signal should be readily detectable as a distinct feature superposed on the resonantly scattered background and will yield information concerning the distribution of H_2 in the upper atmosphere. Observations of Ly-α should provide the distribution of atomic hydrogen down to about 200 km, and the photodissociation process should tell us about the H_2 distribution between 200 and 300 km.

Similarly the helium resonance line at 584 Å can be excited by resonance scattering of the solar 584 Å line by helium in the atmosphere above a level where absorption in H_2 becomes dominant. Radiative transport calculations predict 4.8 R of He 584 Å emission intensity from the entire disk of Jupiter if the He/H_2 ratio is 0.1. The slant emission rate could be as large as 200 R in the absence of absorption; however, there is strong absorption by H_2 at this short wavelength. Therefore, deduction of the height profile of the He density from limb observations appears difficult, but still possible because the integration times needed for a reasonably accurate measurement of He 584 Å airglow are not large. There are 5 to 10 R of galactic He 584 Å radiation that must be subtracted from the planetary limb airglow. However, the background in the proper direction can be determined with great precision during the interplanetary cruise portions of the Voyager Mission.

Emission rates of He can be obtained with high accuracy looking directly at the planets. Again, the amount of radiation emerging from the atmosphere depends upon the helium to hydrogen mixing ratio in the upper atmosphere. If the H_2 distribution with altitude and the height of the homopause are known, then the distribution of He that can produce a given intensity of He 584 Å radiation excited by resonance absorption is uniquely determined. In our discussion of the occultation mode, we show how the H_2 distribution and the location of the homopause may be determined. We also assess the possible contribution to He 584 Å emission from energetic electrons, photoelectrons and precipitating radiation belt particles. The relative intensities of related emissions such as H Ly-α, Ly-β, Ly-γ, Ly-δ can be used to differentiate between the resonance absorption and electron bombardment emission sources.

Airglow observations of a planet or satellite may be profitably begun when the target fills about a quarter of the length of the slit at a distance of about 530 target radii. Jupiter will fill the field of view at a distance of 9.5×10^6 km, or about 8 days before and after encounter. Thus, long integration times needed to achieve good statistical accuracy in defining disk airglow brightness will be available. At Jupiter

encounter, radiation noise will reduce the effective sensitivity of the UVS at less than $14\,R_J, E \pm 12$ hours, so the most useful disk observations will be made further out.

For observations designed to resolve the altitude structure of the bright limb, the 'limb drift' technique will be used; the UVS field of view will be directed at a point above the bright limb with the spectrometer slit aligned tangent to the limb, and the motion of the spacecraft will carry the field of view slowly through the atmosphere. For maximum altitude resolution, it is desirable to be as close to the bright limb as possible. At a distance of $5.5R_J$, the resolution element is the field of view defined by one anode width, 225 km. Since the spacecraft velocity is about 20 km s^{-1}, the field of view moves through the atmosphere at a rate of one resolution element in 11 s. A series of 12 drifts in 20 minutes will produce a signal to noise ratio of about 7 for a 50 km thick slab of atmosphere assuming a typical expected emission profile.

3.2. Occultation measurement

In addition to airglow observations, the second technique for probing the atmosphere is the occultation experiment. For this extremely powerful experiment, the occultation field of the spectrometer is pointed toward the Sun as the spacecraft enters or leaves the shadow behind the planet. The solar spectrum is monitored as a function of tangent ray (Sun–spacecraft line) height. A knowledge of the absolute flux spectrum of the source is not required; the important quantity is the depletion of the source flux as it is absorbed and scattered by the atmosphere. Since all common atmospheric constituents or their photochemical products have strong, characteristic absorption properties in the wavelength range of the UVS, extinction spectra at different altitudes contain information on the composition and vertical distribution of the atmosphere. Atomic hydrogen absorbs continuously below 911 Å, H_2 below 845 Å, and He below 504 Å. The absorption cross-section of CH_4 varies by several orders of magnitude between 1000 and 1700 Å. Recent measurements of this cross-section (Mount *et al.*, 1977) have shown that it is about 200 times smaller than previously accepted values at wavelengths greater than 1475 Å. Since CH_4 absorption will be small at these long wavelengths, a window for viewing other atmospheric hydrocarbons exists in the wavelength range 1500–1700 Å. Both C_2H_2 and C_2H_6 have strong, characteristic absorption cross-sections in this wavelength band. C_2H_2 densities from a model by Strobel (1975) and C_2H_6 densities from Figure 1 have been included in calculations of atmospheric extinction. Figure 7 shows the transmission of Jupiter's atmosphere as a function of wavelength for several altitudes for the model atmosphere having $K \propto M^{-1/2}$ shown in Figure 1. The reference altitude $z = 0$ is at the 10^{16} number density level. The absorption below 845 Å is due primarily to H_2, and may be used to map the density of this constituent from about 475 km to below 350 km. Weaker absorption in the H_2 Lyman and Werner bands between 912 and 1100 Å may extend the lower limit to 250 km. The combination of this type of measurement with the airglow observations of 1607 Å emission will yield the H_2 density distribution down to a level just above the homopause.

Methane absorption is a sensitive indicator of the homopause altitude, and in addition provides information on the temperature profile in the altitude range 0 to 250 km. Because the heavy CH_4 decreases rapidly in density with a scale height of about 2 km above the homopause, absorption in the methane bands shortward of 1480 Å sets in rapidly when the homopause is reached. Thus, the level of the homopause can be defined to within a few kilometers.

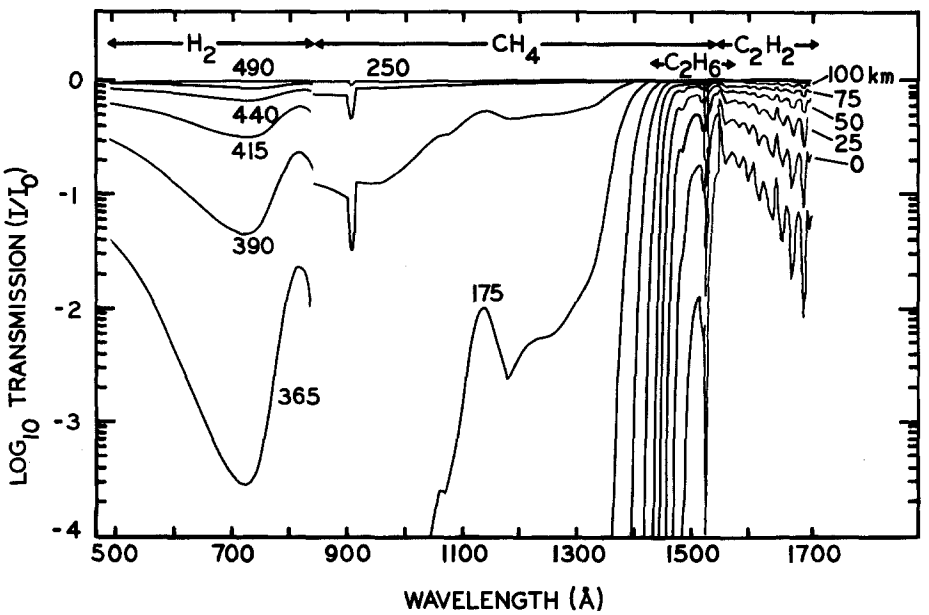

Fig. 7. Transmission of the Jovian atmosphere as a function of wavelength for several tangent ray heights. The altitude increment between curves is 25 km. The calculations are based on the $K \propto M^{-1/2}$ model shown in Figure 1. The locations of the absorption signatures of H_2, CH_4, and C_2H_2 are shown. Weak absorption by C_2H_6 will be measurable in the region indicated, according to this model. The rapid onset of absorption near the homopause (~240 km) by CH_4 at wavelengths shortward of 1480 Å is clearly apparent. Absorption by C_2H_2 can be measured down to about 0 km, where the C_2H_2 number density is about 3×10^9 cm^{-3}. At lower altitudes, Rayleigh scattering by H_2 becomes the dominant absorption mechanism.

With the temperature profile fixed over a wide altitude range by these observations, the H_2 density measured over a portion of it can be predicted over the entire altitude range. Since the homopause height is known, the height profile for the helium distribution may be constructed for any assumed He/H_2 ratio. Only one of these will be capable of reproducing the intensity of the resonantly-scattered He 584 Å emission observed in the airglow experiment. Since the distribution of atomic hydrogen in the upper atmosphere can also be determined from analysis of the Ly-α airglow, a complete atmospheric model showing H_2, H, He and CH_4, as well as

temperature from the 5×10^{15} cm^{-3} density level upward, can be constructed from these observations. There are two primary sources of uncertainty in the determination of the H_2/He ratio. The first of these is the uncertainty in the disk brightness at He 584 Å, which specifies the He density at the homopause. The second is the altitude of the homopause, which must be combined with the H_2 number density profile to obtain the H_2 density at the homopause. Since the atmosphere is mixed below the homopause, the He/H_2 ratio at the homopause is just the required quantity. For an error of 3% in the disk brightness and 2 km in the altitude of the homopause, the inferred He/H_2 ratio will be in error by 14%.

The technique described above assures a determination of the He/H_2 ratio on Jupiter and Saturn, but another approach would be used for Uranus, since recent observations (Rieke and Low, 1974) have indicated that the temperature of Uranus is low enough to freeze CH_4 out of the atmosphere so that absorption by this species cannot be used as a homopause indicator.

The altitude resolution of the occultation technique depends on the spectral integration time and on the spacecraft velocity, which determines the time rate of change of the height of the tangent ray in the atmosphere. During the occultation experiment, the UVS spectral readout time is reduced to only 0.3 sec. Since the line of sight to the Sun or tangent ray will be moving toward the planet at about 10 km sec^{-1}, the basic resolution element in this mode is about 3 km. However, at Jupiter and Saturn the image of the Sun at a given wavelength will cover more than one anode width, and each anode in the image will receive radiation transmitted through a different horizontal 2 arc-min slice of the planetary atmosphere. In the case of Jupiter, the image of the sun is 3.5 anode widths in diameter and at $5R_J$ a single anode samples about 200 km of atmosphere at any instant. The sampling interval of 200 km then moves vertically by 3 km during each sample. To realize the potential 3 km resolution, mathematical deconvolution techniques will be required to extract the details of the altitude profiles. At Uranus, the image of the Sun in a single wavelength will be less than one anode width wide and deconvolution will be simplified somewhat.

Even though sample times must be short because of the high rate of change of the height of the tangent ray, the solar flux is sufficiently high to assure good counting statistics. The detector can accommodate a count rate of 10^4 counts s^{-1} anode^{-1}. This corresponds to a statistical uncertainty of 1% for each one second sample interval. Even better statistics can be achieved by summing several adjacent anodes. Furthermore, over most of the UVS wavelength range the unattenuated solar flux at Jupiter and Saturn will produce well over 10^4 photoelectron events anode^{-1} s^{-1}. The gain of the electron multiplier will be reduced and the detector operated in the pulse integration mode, but the statistical improvement due to the high photoevent rate will be preserved. As the tangent ray moves deeper into the atmosphere and atmospheric absorption decreases the signal, it will be necessary to increase the gain to maintain optimum count rates. Two gain changes will be commanded automatically by the onboard computer system based on real time analysis of the signal

strength in selected wavelength bands. Occultation signal count rates far exceed the maximum radiation-induced noise count rate so that there is no significant loss in statistical accuracy associated with the radiation environment.

3.3. Satellites

Both airglow and occultation techniques can be applied to studies of the satellites as well as the parent planets. The present trajectories include an occultation and close encounter at Titan and other satellites of Jupiter and Saturn may be examined. As typical examples, we discuss here an occultation experiment of Io and airglow observations of Ganymede, for which we have the better model atmospheres but the techniques are common to other targets.

At present, there is no direct observation of the neutral atmosphere of Io. Recent attempts to infer its properties from the observed properties of the ionosphere have led to rather widely differing conclusions (McElroy and Yung, 1975; Johnson *et al.*, 1976). Absorption profiles for an atmosphere taken from McElroy and Yung (1975) are shown in Figure 8. This atmosphere consists of NH_3, N_2, H, and Na. The

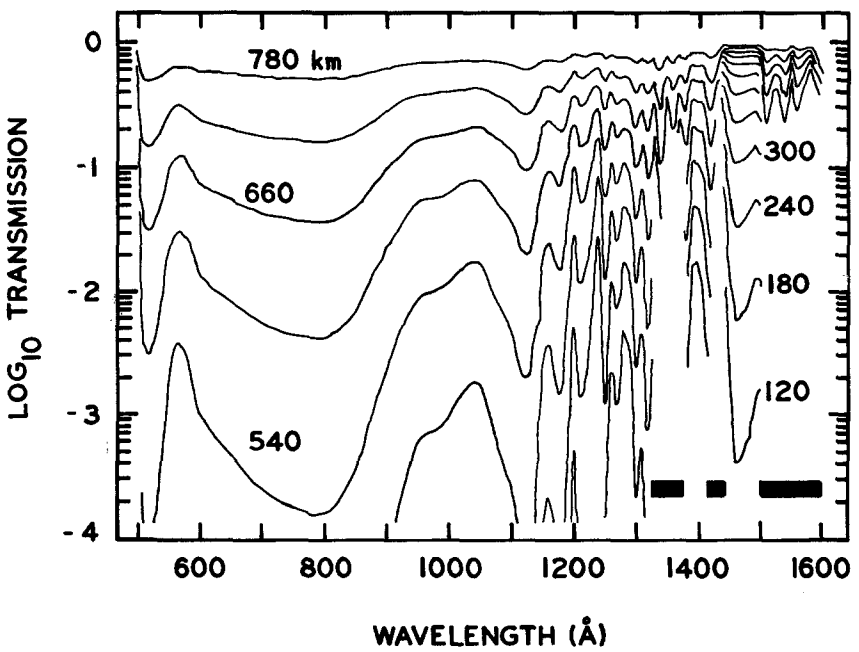

Fig. 8. Transmission of a possible atmosphere of Io as a function of wavelength for several tangent ray altitudes. The altitude increment between curves is 60 km. The major constituent of this atmosphere is NH_3; its absorption signature is obvious. The horizontal bars indicate wavelength ranges for which the variation in transmission at the lower altitudes is too highly structured for inclusion in a graph of this resolution. The large variation in the absorption cross-section of NH_3 over the wavelength range of the UVS enables the occultation technique to probe an altitude range of at least 650 km.

absorption signature of NH_3 is clearly apparent in the wavelength band 1100 to 1500 Å, positively identifying the species. The atmospheric composition and temperature for this model can be mapped over a range of at least 700 km. At an occultation distance of 10^5 km, the resolution element defined by an anode-width is 50 km, the rate of tangent ray height change is about the same as for a planetary occultation, or $3\,\mathrm{km\,s^{-1}}$. These resolution elements may be compared to the expected scale heights of H_2 and NH_3, 1170 and 140 km, respectively. Clearly the spatial resolution is more than adequate to fully characterize the vertical distribution of the atmosphere. Johnson *et al.* (1976) have recently suggested that the neutral atmosphere of Io may be 100 times less dense than the model used to calculate the curves shown in Figure 8. Calculations based on this model show that the two models would be readily distinguishable by the occultation experiment. In a wavelength band near 1100 Å, the altitudes for a transmission of 0.5 differ by 650 km.

For various possible species, we may estimate the minimum surface density for an Io-size satellite required to constitute an atmosphere 'detectable' in the context of this experiment. Based on a maximum absorption of 10%, the required base number density for each of the species NH_3, CH_4, H_2 and O_2 is about $3\times10^7\,\mathrm{cm^{-3}}$. The corresponding pressure for conditions on Io is 1.6×10^{-12} bar.

The dominant atmospheric constituents will be identified by the occultation experiment, but many other constituents will be identified by their emission spectra. Spectral analysis of the emission spectrum coupled with the atmospheric distribution from the occultation experiment, will allow us to infer the electron energy flux and energy distribution due to the flux tube entering Io's atmosphere. This analysis will be similar to that performed on the Earth's atmosphere using the aurora as the atmospheric probe. As mentioned above, further information about Io's flux tube will come from spectral analysis of Jupiter's atmosphere in the region where the flux tube deposition occurs.

Readily detectable auroral activity is expected to occur on Ganymede, as well as Jupiter and the other Galilean satellites. The surface of Ganymede is believed to be primarily water ice, and Yung and McElroy (1977) have provided us with a working model. In this model, the atmosphere is formed by photolysis of H_2O, yielding O_2 as the dominant constituent. Particle detector data from Pioneers 10 and 11 indicate an equatorial electron energy flux of about $300\,\mathrm{erg\,cm^{-2}\,s^{-1}}$ between 0.1 MeV and 1 MeV. For an assumed base pressure of 10^{-3} mbar, most of the energy of the 0.1 MeV electrons will be deposited on the surface rather than in the atmosphere. Secondaries with energies of the order of 30 eV would then excite the atmosphere near the surface, but the intensity due to such a mechanism is difficult to estimate. No direct measurement of the low energy electron flux is available. However, low energy electrons would deliver all their energy to the atmosphere. The amount of energy available above 100 keV suggests a reasonable estimate of energy carried by electrons in the 0.03 to 25 keV region is 10^2 to 10^3 ergs $\mathrm{cm^{-2}\,s^{-1}}$. Such an energy flux is expected to result in intensities of 10^2 to 10^3 R in the atomic oxygen lines at 1304 Å

and 1356 Å. Because of strong absorption by O_2 the atomic oxygen emissions are expected to be observed only from altitudes greater than 100 km. The signature of other minor constituents would also be detected due to the electron bombardment.

Although we will be able to measure the emission spectrum from a satellite, we will be able to get only a crude estimate of the distribution of the intensity over the satellite and will not be able to determine the atmospheric structure. The exception will be Titan with which we will have a close encounter. We will be close to Io also, but we anticipate that the radiation-induced noise at close encounter will preclude a useful measurement of the vertical intensity profiles in the airglow mode. However, weak airglow emissions from Io will be measured at a greater distance when the noise background will be insignificant and the occultation techniques can be used to determine the vertical profiles of gases since the Sun is a source intense enough to dominate the noise from trapped particles. For certain very fundamental questions concerning the primordial conditions in the vicinity of Jupiter and subsequent evolution of the atmospheres and ionospheres, it is not simply the identification of the atmospheric species and measurement of their total column content that is important. One would like to have a definitive knowledge of the distribution of atmospheric gases and temperature profile as well. The UVS is the only Voyager instrument capable of measuring distributions of minor gases and temperature structure in the atmosphere of Io. Most molecular gases have a distinct absorption spectrum. The solar occultation technique which relies on the relative depletion of incoming solar flux on passing through the atmosphere can provide statistically significant measurements of gases whose surface pressures may be as low as 10^{-9} mbar with a height resolution of 3 km. The atmospheric temperature profile can then be deduced from the scale height data.

3.4. Detection of satellite-associated tori

Mapping of the Galilean satellite system to search for and define the spatial extent of gaseous tori can begin quite far from the planet. In the case of Io's hydrogen torus, the observations of Carlson and Judge (1975) and theoretical analysis by Smyth and McElroy (1976) indicate that measurable Ly-α emission should be expected over a significant fraction of the orbit. The extent of the gas cloud perpendicular to the orbital plane is of particular interest. Therefore satellite system mapping will be carried out with the spectrometer slit aligned parallel, as well as perpendicular to, the orbital plane. The orbit of Io extends the length of the slit at a range of 5.6×10^7 km, approximately 50 days from encounter. Long integration times assure the detection of even extremely weak emissions when they provide a signal comparable to 0.1 R from an extended source. For instance, a spectral line emission with an intensity of 10 R over the disk of Io would be detectable from a range of 2×10^7 km, or about 20 days before encounter. The general distribution of brighter emissions can be estimated by deconvolution of the intensity profile as the object becomes comparable in size to the width of the slit and moves slowly through the field of view.

4. Observations of Stellar Sources and Diffuse Emissions

4.1. Comparison to University of Wisconsin OAO-2 Experiments

To evaluate the UVS instrument as a tool for astronomical observations, a comparison to the University of Wisconsin experiments aboard the Orbiting Astronomical Observatory-2 is most appropriate. Instrumental parameters for the two instruments are given in Table I. In our case the limiting magnitude, which was calculated at 1500 Å for a B-star, is considered more from the point of view of possible spectral contamination rather than a working brightness. However, we find that a 7.0 magnitude B-star (1500 Å) will produce about 360 detectable events per anode every hour while we expect less than 10 dark count events per hour. This should be an easily useable signal level. When a similar comparison is made with the University of Wisconsin photometers on OAO-2, we obtain a similar favorable advantage, a calculated improvement of about two orders of magnitude in sensitivity, but a practical advantage of about one order of magnitude.

TABLE I

Comparison of flight instruments for observations of stellar sources

	Wisconsin OAO2 spectrometer[a]	MJS UV spectrometer
Collecting area	265 cm^2	24 cm^2
Spectral increment	10 Å	10 Å
Point source		
Field of view	$8' \times 2'$	$52' \times 2'$
Spectral resolution	10 Å	10 Å
Detectors	1	128
Dark count	1/sec (variable)	3×10^{-3}/sec anode
Limiting magnitude	6	9.5

[a] From Code *et al.*, (1970).

4.2. Astronomy

An exhaustive survey of stellar sources will be made during the cruise phases of the mission. Although signals from stellar sources will be weak, the extremely long observation times available during interplanetary cruise and the low dark count rate of the detector will make stellar observations practical. The sensitivity of the UVS in the context of stellar observations was discussed in Section 4.1. In routine stellar surveys, approximately 8 hours of observation time will be allotted to each target. The coarse cruise phase limit cycle of the scan platform pointing will move the target in and out of the UVS field of view, so that both background and source spectra will be obtained. Limit cycle error signals will be available at 4 sec intervals so that effects of target motion in the field of view can be accounted for during analysis of the data with an accuracy of about 0.01°.

4.3. Diffuse cosmic background

Observations of the high galactic latitude cosmic background radiation will be difficult due to the weak signals expected. However, a flux of 1000 photons $cm^{-2}\,s^{-1}\,sr^{-1}\,Å^{-1}$ at 1500 Å will produce about 30 counts $anode^{-1}\,hr^{-1}$, which should be readily detectable against an intrinsic detector background of less than 10 counts $anode^{-1}\,hr^{-1}$. Interpretation of the data will be complicated by background H Ly-α from the interplanetary medium scattered in the instrument into all wavelength channels. Furthermore, the possibility of the presence of stars in the field must be carefully evaluated. However, we have the advantage of long, undisturbed observing periods; a hundred hours is practical, which will make the spectral signature detectable. A systematic series of observations will be designed to sort out contributions from the various possible sources.

4.4. Interplanetary emissions (He and H maps)

Observations of the resonantly scattered He 584 Å and H Ly-α emission from the interstellar medium will be carried out to construct a map of the celestial sphere in these wavelengths. Since the emission intensities are relatively large (70–400 R for H Ly-α, and 4–15 R for He 584), the mapping is straightforward. It will be performed at intervals of approximately six months during regularly scheduled spacecraft roll calibration maneuvers. Between each revolution of the spacecraft, the instrument field of view will be stepped in elevation so that a major portion of the celestial sphere is swept out in a short time.

Acknowledgment

The Kitt Peak National Observatory is operated by the Association of Universities for Research in Astronomy, Inc., under contract with the National Science Foundation. This work was supported by the Jet Propulsion Laboratory, California Institute of Technology, under NASA contract NAS 7-100.

References

Atreya, S. K. and Donahue, T. M.: 1976, in T. Gehrels (ed.), *Jupiter*, University of Arizona Press, Tucson, Arizona, p. 304.
Barker, E. S.: 1977, 'Copernicus Observations of Solar System Objects', *Bull. Am. Astron. Soc.*, (in press).
Beutler, H. G.: 1945, *J. Opt. Soc. Am.* **35**, 311.
Blum, P. W., Pfleiderer, J. and Wulf-Mathies, G.: 1975, *Planet. Space Sci.* **23**, 93.
Broadfoot, A. L., Clapp, S. S., and Stuart, F. E.: 1977a, *Space Sci. Inst.* **3**, 199.
Broadfoot, A. L., Clapp, S. S., and Stuart, F. E.: 1977b, *Space Sci. Inst.* **3**, 209.
Broadfoot, A. L. and Sandel, B. R.: 1977 *Appl. Opt.* **16**, (in press).
Carlson, R. W. and Judge, D. L.: 1974, *J. Geophys. Res.* **79**, 3623.
Carlson, R. W. and Judge, D. L.: 1975, *Icarus* **24**, 395.
Code, A. D., Houck, T. E., McNall, J. F., Bless, R. C., and Lillie, C. F.: 1970, *Astrophys. J.* **161**, 377.
Fjeldbo, G., Kliore, A., Seidel, B., Sweetnam, D., and Woiceshyn, P.: 1976, in T. Gehrels (ed.) *Jupiter*, University of Arizona Press, Tucson, Arizona, p. 238.

French, R. G. and Gierasch, P. J.: 1974, *J. Atmos. Sci.* **31**, 1707.
Giles, J. W., Moos, H. W., and McKinney, W. R.: 1976, *J. Geophys. Res.* **81**, 5797.
Goldreich, P. and Lynden-Bell, D.: 1969, *Astrophys. J.* **156**, 59.
Johnson, T. V., Matson, D. L., and Carlson, R. W.: 1976, *Geophys. Res. Lett.* **3**, 293.
Lampton, M., Margon, B., Paresce, S., Stern, R., and Bowyer, S.: 1976, *Astrophys. J. (Lett.)* **203**, L71.
McElroy, M. B. and Yung, Y. L.: 1975, *Astrophy. J.* **196**, 227.
Moos, H. W., Fastie, W. G., and Bottema, M.: 1969, *Astrophys. J.* **155**, 887.
Mount, G. H., Warden, E. S., and Moos, H. W.: 1977, *Astrophys. J. (Lett.)* (in press).
Pilcher, C. B.: 1976, *Astrophys. J.* **207**, 646.
Rieke, G. H. and Low, F. J.: 1974, *Astrophys J. (Lett.)* **193**, L147.
Rottman, G. J., Moos, H. W., and Freer, C. S.: 1973, *Astrophys. J.* **184**, L89.
Smyth, W. B. and McElroy, M. B.: 1977, 'The Sodium and Hydrogen Gas Clouds of Io' *Planet. Space Sci.* (submitted).
Strobel, D. F.: 1975, *Rev. Geophys. Space Phys.* **13**, 372.
Trafton, L., Parkinson, T., and Macy, W.: 1974, *Astrophys. J. (Lett.)* **190**, L85.
Trafton, L. and Macy, W.: 1975, *Astrophys. J. (Lett.)* **202**, L155.
Veverka, J., Elliott, J., Wasserman, L. and Sagan, C.: 1974, *Astron. J.* **179**, 73.
Wadsworth, F. L. O.: 1896, *Astrophys. J.* **3**, 54.
Yung, Y. L. and McElroy, M. B.: 1977, *Icarus* **30**, 97.